Mon. Not. R. Astron. Soc. **000**, 000–000 (2000)

Multiphase Smoothed-Particle Hydrodynamics

Benedict W. Ritchie⋆ and Peter A. Thomas
Astronomy Centre, School of Chemistry, Physics and Environmental Science, University of Sussex, Falmer, Brighton BN1 9QJ

Accepted —. Received —; in original form —

ABSTRACT

We adapt the Smoothed-Particle Hydrodynamics technique to allow a multiphase fluid in which gas particles of widely differing density may be freely intermixed. Applications include modelling of galaxy formation and cooling flows.

Key words: methods: numerical - hydrodynamical simulation - galaxies: formation - cooling flows

1 INTRODUCTION

Since its introduction more than two decades ago by Lucy (1977) and Gingold & Monaghan (1977), Smoothed-Particle Hydrodynamics (SPH) has become one of the standard techniques for modelling astrophysical fluid flow (e.g. Evrard 1988; Hernquist & Katz 1989, hereafter HK89; Thomas & Couchman 1992; Steinmetz & Müller 1993; Couchman, Thomas & Pearce 1995, hereafter CTP95; Shapiro et al. 1996). SPH is fully Lagrangian, with the particles themselves being the framework on which the fluid equations are solved, and so there is no grid to constrain the dynamic range or geometry of the system being modelled. This is of particular importance for phenomena involving the growth of gravitational fluctuations, such as cosmological structure formation (Bertschinger 1998) and star formation (Bhattal et al. 1998), and in an adaptive form (Wood 1981; Nelson & Papaloizou 1994) the SPH algorithm will follow the wide range of densities encountered without difficulty. In contrast, the computational demands imposed by the storage and evaluation of complex refined grids restrict Eulerian finite-difference methods (e.g. the Piecewise-Parabolic Method of Collela & Woodward 1984) to poor resolution, and to date the best three-dimensional Eulerian simulations of galaxy formation have a gas resolution of $\sim 300 - 500$ kpc (Blanton et al. 1999). SPH can be easily integrated with a range of N-body gravity solvers such as the tree algorithm used by HK89 and the Adaptive Particle-Particle, Particle-Mesh (AP^3M) algorithm of Couchman (1991).

However, SPH is not without its problems. The need for an artificial viscosity means that SPH resolves shocks poorly in comparison with finite-difference methods. Pairwise artificial viscosities (Monaghan & Gingold 1983) generally give the sharpest resolution of shocks, but also introduce a large shear viscosity unless correction terms are used (Balsara 1995). There is some concern that these terms further degrade the shock capturing ability of SPH (Navarro & Steinmetz 1997; Thacker et al. 1998, hereafter T98). While it is possible to add a *physical* viscosity to SPH and solve the Navier-Stokes equations directly (e.g. Flebbe et al. 1994), the relatively simple SPH interpolation method is quite sensitive to particle disorder and tends to give large errors in the higher-order dissipative terms. Boundary conditions are also difficult to implement in SPH, and do not sit naturally with the method. Generally boundaries are either periodic or situated far from the region of interest, and SPH is unsuitable for simulations in which complex boundary conditions are of critical importance.

Standard implementations of SPH also have a limited ability to resolve steep density gradients, and a number of numerical problems can occur when particles are close to, but not physically part of, a region of higher density. These arise because the usual formulation of SPH assumes that there is a small density variation across the smoothing kernel of each particle. However, this is not true in many situations in which SPH is commonly used. In simulations of galaxy formation, for example, thermal instability causes cold, dense clumps to form within halos of hot gas, and density contrasts of several orders of magnitude can occur within the typical smoothing length of the halo gas. Current implementations of SPH will overestimate the density of the halo gas, leading to the gas cooling excessively and accreting on to the cold clump (T98). Tittley, Couchman and Pearce (1999, hereafter TCP99) have also shown that the drag exerted on these protogalaxies by the intracluster medium can be seriously overestimated. These problems are thought to contribute to the overmerging commonly seen in simulations of structure formation including gas (Frenk et al. 1996).

We wish to extend the method to cope with these problems, along with multiphase fluids, such as the intracluster medium or cooling flows, in which there is no correlation

⋆ Email: B.W.Ritchie@sussex.ac.uk

between the density of neighbouring particles. To do this, we make two changes to the standard implementation of SPH. Firstly, particles no longer have to maintain a fixed number of neighbours, as is required by the algorithm of HK89, and instead the smoothing length is adjusted to keep a density-weighted quantity constant (see Section 2.1). This prevents the smoothing length of low density particles from decreasing as they approach a high density region. Secondly we make the assumption that pressure, not density, is constant across the smoothing kernel. We then summate the local pressure at each particle and calculate the local density from the equation of state. This is a reasonable approach to take when the cooling time of the gas is greater than the local dynamic time, where a local pressure equilibrium can be expected even when the local density gradient is steep. It will *not* be true in the presence of shocks (although neither is the assumption that density is smoothly varying). As we will see in section 3.1, however, there is no evidence that the shock capturing ability of SPH is degraded.

The layout of the paper is as follows. In section 2 we detail our new implementation of SPH. In Section 3 we present the results of a number of tests of the new method, and compare the performance with results produced using the SPH implementations of CTP95 and T98. This is followed in Section 4 by a discussion of our results.

2 SPHM: METHODOLOGY

In SPH the fluid is represented by particles of known mass, m_i, and specific energy, ϵ_i. Other properties must be inferred by averaging over a smoothing sphere that typically extends to enclose a fixed number, $N_{\rm SPH}$, of particles. For a continuous distribution, the average value of some quantity A at the location of particle i would be

$$\langle A_i \rangle = \int A(\mathbf{r})\, W(\mathbf{r}-\mathbf{r_i})\, \mathrm{d}V \tag{1}$$

where W is the smoothing kernel. In SPH the integral is replaced by a sum:

$$\langle A_i \rangle = \sum_j \frac{m_j}{\rho_j} A_j W_{ij} \tag{2}$$

that extends over all particles, j, within the smoothing sphere. ρ_j is the density of particle j and so m_j/ρ_j is its volume.

For consistency, we require

$$\sum_j \frac{m_j}{\rho_j} W_{ij} = 1 \tag{3}$$

although this will only be true in a statistical sense.

There are apparently two deficiencies in Equation 2. Firstly, it is circular in that A appears on both sides, and secondly it seems to require the value of ρ_j, which is not known in advance. However, it is possible to circumvent these problems by formulating SPH such that A is always a multiple of density and a known quantity.

Where expressions arise involving derivatives, we use the divergence theorem to transfer the derivative onto the smoothing kernel as follows:

$$\langle \nabla A_i \rangle = \int \nabla A\, W\, \mathrm{d}V = -\int A \nabla W\, \mathrm{d}V \tag{4}$$

$$\langle \nabla . \mathbf{A}_i \rangle = \int \nabla . \mathbf{A}\, W\, \mathrm{d}V = -\int \mathbf{A} . \nabla W\, \mathrm{d}V \tag{5}$$

2.1 The smoothing length

The smoothing length in SPH is usually defined in terms of the radius of a sphere, centred on the particle in question, that encloses a fixed number of neighbours. One can either search for such a radius on each time-step, a time-consuming process, or accept an estimate based on the number of neighbours found on the previous step:

$$h_i \leftarrow h_i \left[\alpha + (1-\alpha) \left(\frac{N_{\rm SPH}}{N_i} \right)^{\frac{1}{3}} \right], \tag{6}$$

where N_i is the actual number of neighbours and $N_{\rm SPH}$ is the desired number. α is a convergence parameter: for a uniform distribution, choosing $\alpha = 1$ returns the correct value of h_i on the next step. Where large density contrasts are present, however, α must be reduced to avoid overshooting and convergence is much slower. We use a convergence parameter $\alpha = 0.4$ and $N_{\rm SPH} = 32$.

For the extreme density contrasts we envisage, T98 have shown that N_i can oscillate between values which are alternately too low and too high. They solve this problem both by giving lower weight to particles at the extreme edge of the smoothing sphere, and by the introduction of a more sophisticate convergence algorithm.

In this paper, we suggest a simpler approach that uses a neighbour count weighted as follows:

$$N_i = \sum_j w_{ij} = \sum_j \frac{2\bar{\rho}_i}{\bar{\rho}_i + \rho_j}, \tag{7}$$

where $\bar{\rho}_i$ is the mean density at particle i and the sum extends over all neighbours within the smoothing sphere. Note that:

(i) For a uniform distribution in which $\bar{\rho}_i = \rho_j$, then $w_{ij} = 1$ and N_i is simply equal to the number of neighbours.
(ii) Particles do not notice neighbours with a much greater than average density ($w_{ij} \sim 0$ for $\bar{\rho}_i \ll \rho_j$). This prevents the common instability whereby changing the radius of the smoothing sphere so as to include or exclude a high-density clump can dramatically change the number count.
(iii) Neighbours with a lower than average density count at most double ($w_{ij} \sim 2$ for $\bar{\rho}_i \gg \rho_j$). It would be possible to limit w_{ij} to have a maximum value of unity, but this seems unnecessary.

2.2 Evaluation of the density

In multiphase SPH, it is important to distinguish between the density of a particle, ρ_i, and the mean density in the neighbourhood of a particle, $\bar{\rho}_i$. The SPH estimate for the latter is

$$\langle \bar{\rho}_i \rangle = \sum_j m_j W_{ij}, \tag{8}$$

where

$$W_{ij} = \frac{1}{h_{ij}^3} W(r_{ij}/h_{ij}), \tag{9}$$

r_{ij} is the separation of particles i and j, $r_{ij} = |\mathbf{r}_i - \mathbf{r}_j|$, and h_{ij} is the smoothing length. There are several possible forms for W. Throughout this paper, we use the standard form described in Thomas & Couchman (1992).

The choice of h_{ij} determines the size of the region over which the density is to be averaged. Many authors take h_{ij} to be a symmetric function (for example the harmonic average) of h_i and h_j. We prefer to set $h_{ij} = h_i$. This has the advantages that we know in advance exactly how far we have to search and always have the same (weighted) number of neighbours within the smoothing region.

The mean density of the gas can vary between high- and low-density regions. The pressure of the gas is expected to be a much smoother quantity because (excluding shocks) the sound-crossing time is shorter than the flow time across a smoothing sphere. Hence we define the density of a particle in terms of the pressure:

$$\langle \rho_i \rangle = \frac{3\langle P_i \rangle}{2\epsilon_i} = \frac{\sum_j m_j \epsilon_j W_{ij}}{\epsilon_i}. \tag{10}$$

Note that a cold, high-density clump of particles will contribute a lot of terms to the sum, but each of these will be given a low weight due to the presence of the ϵ_j term. This is in contrast with the expression for the mean density, Equation 8. The consistency condition, Equation 3, becomes

$$\sum_j \frac{2 m_j \epsilon_j W_{ij}}{3\langle P_j \rangle} = 1 \tag{11}$$

which will be true if the pressure is slowly-varying, as we have assumed.

2.3 The equation of motion

In the absence of artificial viscosity, heating and radiative cooling, the equation of motion for a parcel of gas is simply

$$\frac{\mathrm{d}\mathbf{v}}{\mathrm{d}t} = -\frac{\nabla P}{\rho}. \tag{12}$$

In the same spirit as above, we require an estimate of ∇P that does not depend upon the number density of particles. This is

$$\langle \nabla P_i \rangle = \frac{2}{3} \sum_j m_j \epsilon_j \nabla_i W_{ij}. \tag{13}$$

It is common practice to use the following identity

$$\frac{\nabla P}{\rho} = \nabla \left(\frac{P}{\rho} \right) + \frac{P}{\rho^2} \nabla \rho \tag{14}$$

to symmetrise the pressure force. This expression is not suitable here, both because we are envisaging abrupt changes in density (so that $\nabla\rho$ is undefined) and because the estimator for P/ρ^2 depends upon the density of the particles. Equation 14 is obtained using the general identity

$$\frac{\nabla P}{\rho} = \frac{P}{\rho^\sigma} \nabla \left(\frac{1}{\rho^{1-\sigma}} \right) + \frac{1}{\rho^{2-\sigma}} \nabla \left(\frac{P}{\rho^{\sigma-1}} \right) \tag{15}$$

(Monaghan, 1992) and using $\sigma = 1$ gives an alternative identity that at first sight seems a little bizarre:

$$\frac{\nabla P}{\rho} = \frac{\nabla P}{\rho} + \frac{P}{\rho} \nabla 1. \tag{16}$$

This leads to the symmetric estimator for the force on particle i,

$$\langle \mathbf{f}_i \rangle = \sum_j \frac{2}{3} m_i m_j \left[\frac{\epsilon_j \nabla_i W_{ij}}{\langle \rho_i \rangle} + \frac{\epsilon_i \nabla_i W_{ij}}{\langle \rho_j \rangle} \right]. \tag{17}$$

If we ignore the distinction between W_{ij} and W_{ji} then this can be written as

$$\langle \mathbf{f}_i \rangle = \sum_j \big(\mathbf{f}_{ij} - \mathbf{f}_{ji} \big), \tag{18}$$

where

$$\mathbf{f}_{ij} = \frac{2}{3} m_i m_j \frac{\epsilon_j \nabla_i W_{ij}}{\langle \rho_i \rangle}. \tag{19}$$

The first set of terms in Equation 18 is evaluated when calculating the SPH properties for particle i; the second set is accumulated in stages when calculating the properties of the neighbours.

Note that the only change from the usual SPH formalism is that ϵ_i and ϵ_j have exchanged places in Equation 17. However, this change means that the force on particle i is dependent only upon the local pressure gradient and not upon the density of its neighbours.

2.4 Conservation of energy

Conservation of energy is ensured by equating the heating to the $P\mathrm{d}V$ work done:

$$\frac{\mathrm{d}\epsilon}{\mathrm{d}t} = -\frac{P}{\rho} \nabla.\mathbf{v}. \tag{20}$$

By making use of the identity

$$\nabla.\mathbf{v} = \nabla.\Delta\mathbf{v}, \tag{21}$$

where $\Delta\mathbf{v} = \mathbf{v} - \mathbf{v}_i$, this can be put into a variety of forms. For example,

$$\frac{\mathrm{d}\epsilon}{\mathrm{d}t} = -\frac{\nabla.(P\,\Delta\mathbf{v})}{\rho} + \frac{\Delta\mathbf{v}.\nabla P}{\rho} \tag{22}$$

gives

$$\left\langle \frac{\mathrm{d}\epsilon_i}{\mathrm{d}t} \right\rangle = \frac{2}{3} \sum_j \frac{m_j \epsilon_j \mathbf{v}_{ij}.\nabla_i W_{ij}}{\langle \rho_i \rangle} = \frac{1}{m_i} \sum_j \mathbf{f}_{ij}.\mathbf{v}_{ij}, \tag{23}$$

where $\mathbf{v}_{ij} = \mathbf{v}_j - \mathbf{v}_i$—the second term has vanished because it contains $\mathbf{v}_{ii}$ which is identically zero. Using

$$\frac{\mathrm{d}\epsilon_i}{\mathrm{d}t} = -\frac{P \nabla.\Delta\mathbf{v}}{\rho}, \tag{24}$$

we obtain an alternative expression

$$\left\langle \frac{\mathrm{d}\epsilon_i}{\mathrm{d}t} \right\rangle = \frac{2}{3} \sum_j \frac{m_j \epsilon_i \mathbf{v}_{ij}.\nabla_i W_{ij}}{\langle \rho_j \rangle} = \frac{1}{m_i} \sum_j \mathbf{f}_{ji}.\mathbf{v}_{ji}. \tag{25}$$

Combining Equations 23 and 25, we find that

$$m_i \left\langle \frac{\mathrm{d}\epsilon_i}{\mathrm{d}t} \right\rangle = \frac{1}{2} \sum_j \big(\mathbf{v}_{ij}.\mathbf{f}_{ij} + \mathbf{v}_{ji}.\mathbf{f}_{ji} \big), \tag{26}$$

where $\mathbf{f}_{ij}$ is the pairwise force given in Equation 19.

Any of Equations 23, 25, or 26 (or any similarly derived equation) may be used as an estimator of $\mathrm{d}\epsilon/\mathrm{d}t$ (and hence, by rearrangement of Equation 20, for $\nabla.\mathbf{v}$). Under most conditions, the performance of the three equations is indistinguishable, and standard tests of SPH cannot tell them apart.

However, when large temperature variations are present the double-sided form can lead to a large scatter in particle entropy. We use Equation 23 here.

2.5 Artificial viscosity

In the presence of shocks, we require a mechanism to convert relative motion into heat. In SPH, this is achieved via an artificial pressure, Q, that is added to the usual one in regions of convergent flow. This has the effect of replacing P by $P+Q$ in Equations 12 and 20. In the current method, we replace $\mathbf{f}_{ij}$ in Equations 18 and 25 with $\mathbf{f}_{ij}+\mathbf{g}_{ij}$, where

$$\mathbf{g}_{ij} = \mathbf{f}_{ij}\mathcal{M}_{ij}(\beta\,\mathcal{M}_{ij}+\alpha) \tag{27}$$

(Monaghan & Gingold 1983; T98). Here the pairwise Mach number

$$\mathcal{M}_{ij} = \begin{cases} 0, & \mathbf{r}_{ij}.\mathbf{v}_{ij} > 0 \\ \frac{h_i|\mathbf{r}_{ij}.\mathbf{v}_{ij}|}{c_{ij}\,(r_{ij}^2+0.01h_i^2)}, & \mathbf{r}_{ij}.\mathbf{v}_{ij} < 0 \end{cases} \tag{28}$$

the particle separation, $r_{ij} = |\mathbf{r}_{ij}| = |\mathbf{r}_j - \mathbf{r}_i|$, and the sound speed

$$c_{ij} = \frac{c_i + c_j}{2} \tag{29}$$

where

$$c = \sqrt{(10\epsilon/9)}. \tag{30}$$

We adopt the values $\alpha = 1$, $\beta = 2$. The use of c_{ij} in Equation 28 rather than c_i helps to limit the degree to which cold particles shock against dense clumps.

In addition, a shear-correcting term (Balsara 1995) can be applied to limit the damping of shear flows. Following Steinmetz (1996) we use

$$\mathcal{M}_{ij} \rightarrow \tilde{\mathcal{M}}_{ij} = \mathcal{M}_{ij}k_i \tag{31}$$

where

$$k_i = \frac{|\langle\nabla.\mathbf{v}\rangle_i|}{|\langle\nabla.\mathbf{v}\rangle_i| + |\langle\nabla\times\mathbf{v}\rangle_i| + 0.0001c_i/h_i}. \tag{32}$$

For compressional flows $k = 1$ and $\mathcal{M}_i$ is unchanged, while in shearing flows $k \rightarrow 0$ and the artificial viscosity vanishes. The tests presented in this paper do not apply this correction term.

2.6 Cooling

In the presence of artificial viscosity and cooling, the Equation of Energy Conservation becomes

$$\frac{\mathrm{d}\epsilon}{\mathrm{d}t} = -\frac{P+Q}{\rho}\,\nabla.\mathbf{v} - \xi, \tag{33}$$

where ξ is the emissivity (the emission rate per unit volume). The cooling function is interpolated from Sutherland & Dopita (1993). To minimise problems of cooling during shock-heating (see Hutchings & Thomas 1999), we allow the gas to cool only at the end of a time-step after the artificial viscosity term has been applied. The cooling is assumed to occur at constant density (the time-step ensures that this condition is approximately satisfied), as described in Thomas & Couchman (1992).

3 SPHM: TESTS

The tests discussed in the following sections were carried out using Hydra† (Couchman, Thomas and Pearce, 1995), an AP^{3}M+SPH code modified to use the SPH method detailed in this paper. The simulations were performed on single-processor Sun and Intel workstations.

3.1 Shock Tube

A standard test of gas dynamical codes is the Sod Shock (Sod 1978), which has been applied to SPH by many authors (e.g. Monaghan & Gingold 1983; Rasio & Shapiro 1991; T98). Analytic results are given by Hawley, Smarr & Wilson (1984) and Rasio & Shapiro (1991). In the Sod Shock two regions of gas with different densities are brought into contact, resulting in a shock wave propagating into the low-density gas and a rarefaction wave propagating into the high density gas. Between these two regions is a contact discontinuity, where the pressure is constant but the density jumps. The Sod shock is a single-phase problem, but is included to test whether our assumption that pressure is smoothly varying degrades the shock-capturing ability of SPH. Following T98 we use the initial conditions

$$\begin{array}{llll} \rho_l = 4 & P_l = 1 & v_l = 0. & \text{for } x < 0 \\ \rho_r = 1 & P_r = 0.1795 & v_r = 0. & \text{for } x \geq 0 \end{array} \tag{34}$$

giving a shock Mach number $\mathcal{M} \sim 1.4$. Both regions are allowed to evolve at constant temperature before being brought into contact, to allow the gas to relax to a physically realistic initial state. A total of 7343 equal mass particles are used, and we use an ideal gas equation of state.

Thirty timesteps are required to reach the state shown in Figure 1, by which time the shock front has moved around 13 code units to the right. Both the shock and the contact discontinuity are broadened over a range $\Delta x \approx 3h$. The results are in good agreement with the analytic solutions, although in common with other implementations of SPH the gradient of the rarefaction wave is too shallow and there is a 'blip' in the pressure at the contact discontinuity (e.g. Gingold & Monaghan 1983). Flow is reasonably smooth, and there is no post-shock ringing. Figure 2 compares the results from our code with those of T98 and CTP95. There is very little difference between the three implementations, although the CTP95 implementation produces a broader shock than the other two codes. This is due to the choice of artificial viscosity — CTP95 uses an artificial viscosity based on the divergence of the local velocity field, which is shown in T98 to be worse at shock capturing than the pairwise artificial viscosity used in T98 and our code. All three implementations model the rarefaction wave similarly, as viscous terms do not apply in expanding regions.

With $\mathcal{M}\sim$1.4, this test represents a fairly weak shock. A strong adiabatic shock presents a more demanding test, as the pressure jump across the shock, and hence the Mach number, are infinite. In this case the jump conditions are

† This code is in the public domain and can be downloaded from http://hydra.mcmaster.ca/.

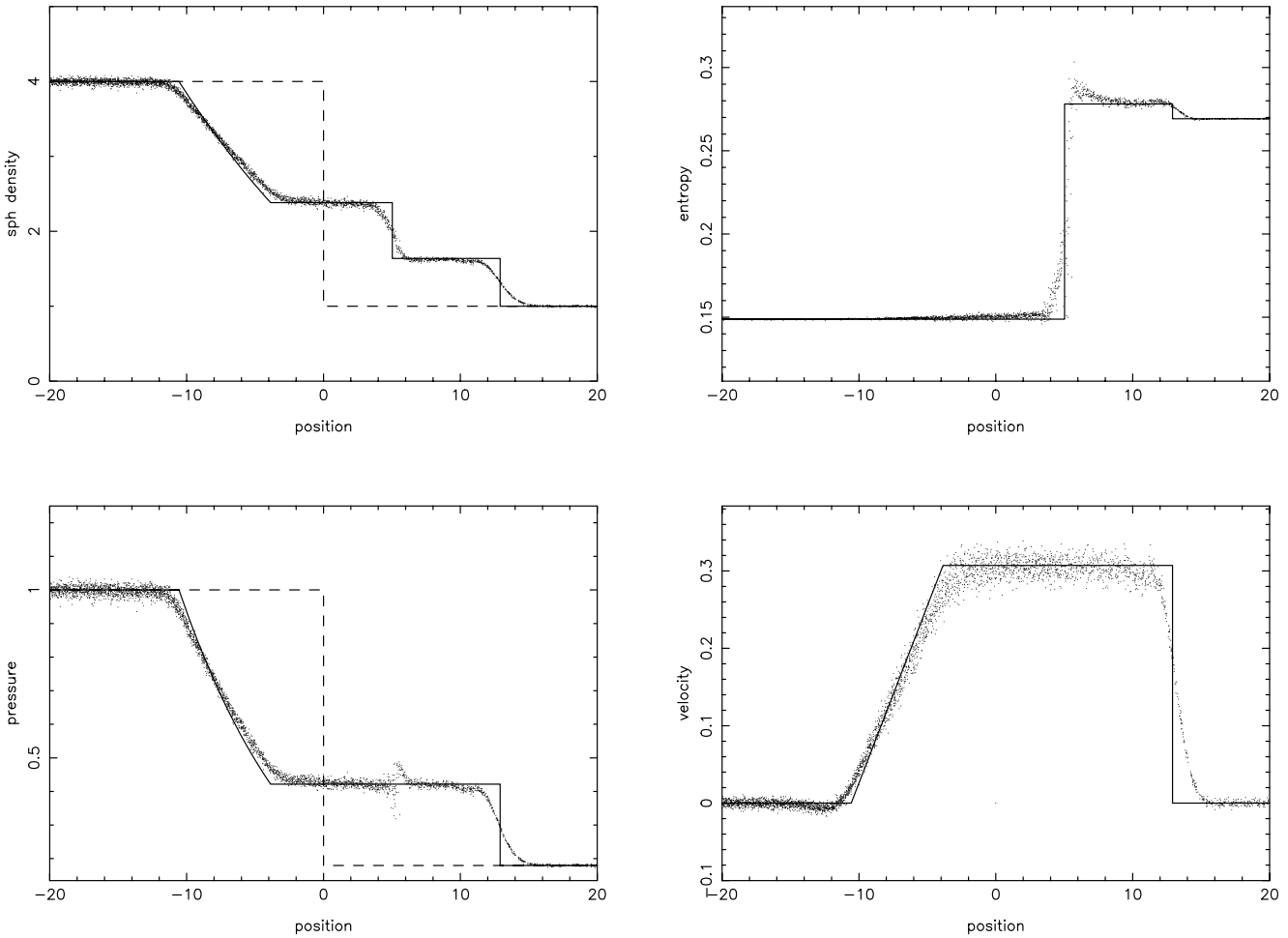

Figure 1. Results from the Sod Shock test after 30 time-steps. The variation in density, pressure, velocity and the entropic function $A(s) = \varepsilon/\rho^{(\gamma-1)}$ across the shock are shown. Analytic solutions are shown as solid lines, and the initial pressure and density profiles defined in equation 34 are shown as dashed lines.

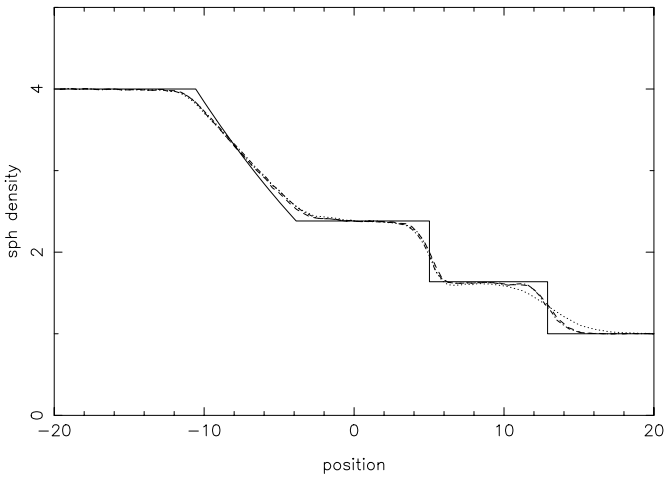

Figure 2. A comparison between the results from this code (dashed line) and those of CTP95 (dotted line) and T98 (dotted-dashed line). The shock front is at $x \approx 13$

$$\begin{array}{llll} \rho_l = 1 & P_l = 0 & v_l = 1.333 & \text{for } x < 0 \\ \rho_r = 4 & P_r = 1.333 & v_r = 0.333 & \text{for } x \geq 0 \end{array} \tag{35}$$

although in our code we require particles to have a minimum temperature, leading to P_l being slightly greater than zero and the Mach number remaining large but finite. The density profile across the shock is shown in Figure 3. The new code is clearly capable of handling such shocks, and while some post-shock oscillation is visible it is not noticeably different from the results obtained from the other codes. As the performance of our code is so close to that of T98 there is no evidence that our assumption that pressure is smoothly varying has affected the shock-capturing ability of the code.

3.2 A multiphase smoothing length update algorithm

In adaptive forms of SPH, the smoothing length h is updated each time-step so that the particle has a constant or near-constant number of neighbours (e.g. the method of HK89). When the density is constant or slowly varying this approach works well, but steep density gradients cause a number of problems. T98 have shown that the HK89 algorithm can

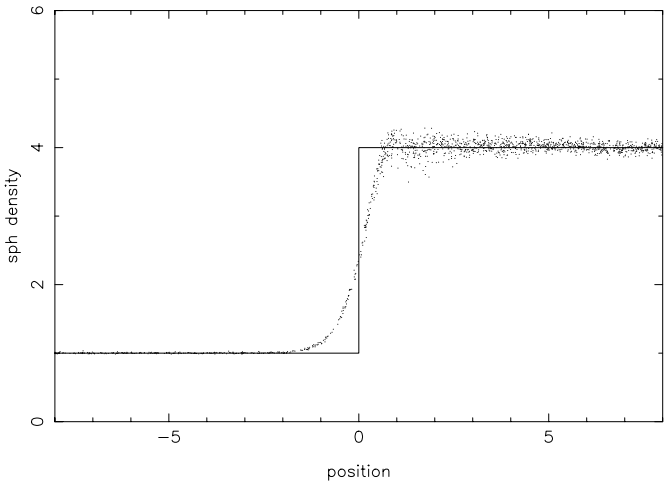

Figure 3. The density jump across a strong adiabatic shock. Results from this code are shown.

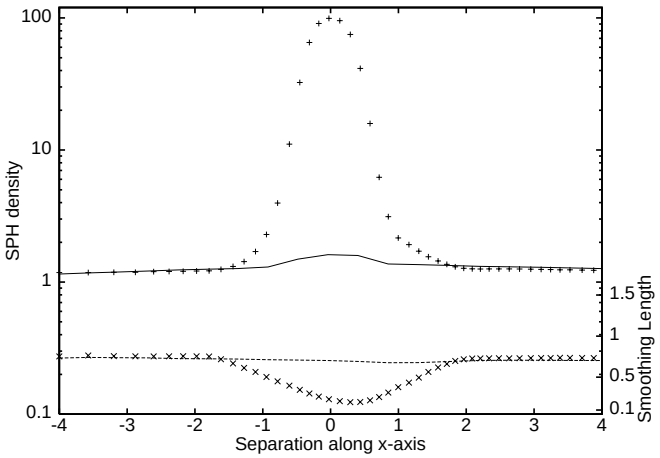

Figure 4. Change in the smoothing length h and the SPH estimate of the density ρ as a particle in a stream of hot gas moves past a dense clump, grazing the surface of the clump at closest approach. The central density of the clump is 200 times that of the surrounding gas, with the temperature set so that the clump is in pressure equilibrium with its surroundings. The density calculated by the multiphase method is shown as a solid line, with the smoothing length h shown as a dashed line. The density calculated by the standard method is shown as a '+' symbol and the smoothing length as a '×' symbol.

become unstable under such conditions, and there is a general tendency for arbitrarily steep density gradients to be smoothed over distances representative of the local value of h, resulting in particles close to, but not physically in, such gradients having their densities incorrectly estimated. This is a cause for concern in simulations of cosmological structure formation, where cold dense clumps of gas - galaxies - form within diffuse halos of hotter gas. The density of halo gas can be overestimated by an order of magnitude or more in the steep density gradients around the largest galaxies, leading to the gas cooling radiatively and being accreted by the galaxy, when physically the two phases would be effectively decoupled. Kay et al. (1999) find that, in their simulations of cluster formation, cD galaxies can form with masses in excess of $5 \times 10^{11} h^{-1}$M at $z = 0$, which, while not impossibly large, is unlikely in the volume of the Universe they consider. Excessive cooling is shown to be responsible, as decoupling the hot and cold phases (Pearce et al. 1999) reduces the final mass of the galaxy to a more reasonable value.

The smoothing of steep density gradients is a consequence of the Lagrangian nature of SPH and the use of Equation 8 for estimating the density. Particles act as tracers of the underlying mass distribution, and a high-density region will therefore contain more particles than a region of lower density. A particle close to a dense clump of gas will need to search little further than the edge of the dense region to find its required number of neighbours, and, as for a fixed number of neighbours $\rho \propto h^{-3}$, the estimated density will be dependent on the separation from the clump. Our approach seeks to avoid this problem by weighting the neighbour count using equation 7, so that a low-density particle close to a dense clump will assign a very low weight to particles in the clump and will search for neighbours as if the clump was not present. While this may result in a particle having many more neighbours than the number sought by the HK89 algorithm (normally in the range 32 — 72), in a region of approximate pressure equilibrium high density particles will be at low temperature and will contribute a negligible amount to Equation 10, the estimate of the pressure used for calculating the particle density.

The benefits of our approach can be seen in Figure 4. Here we plot the change in smoothing length and the SPH estimate of the density as a hot gas particle moves past a cold, dense clump, grazing the surface of the clump at closest approach. The clump has a central density 200 times that of the surrounding gas, with temperatures set so that the two phases are in pressure equilibrium. For the purposes of this test all inter-particle forces have been turned off, so that the particles move at constant velocity. Initially, the density of the hot particle is ~ 1.15 and the smoothing length $h \sim 0.75$, both in code units. In the standard implementation of SPH once the smoothing kernel of the hot particle overlaps the cold clump it finds many more than the desired number of neighbours and the HK89 algorithm starts to decrease the smoothing length in response, with h reaching a minimum of ~ 0.19 shortly after closest approach (this delay is due to the convergence parameter α in Equation 6 limiting the rate at which h_i can change). There is a corresponding increase in the estimate of the density, which peaks slightly earlier at $\rho \sim 97$, an overestimate of almost two orders of magnitude. These values of h and ρ are typical of cold particles on the surface of the clump, indicating that despite the large difference in temperature between the hot and cold particles the standard implementation of SPH treats them identically.

In contrast, our method keeps the smoothing length virtually constant throughout the transit, with h decreasing to ~ 0.72 shortly after closest approach and ρ only increasing from 1.15 to 1.61. This small increase in density is due to the smoothing kernel of the hot particle overlapping the entire clump when the particle gets to within a distance of

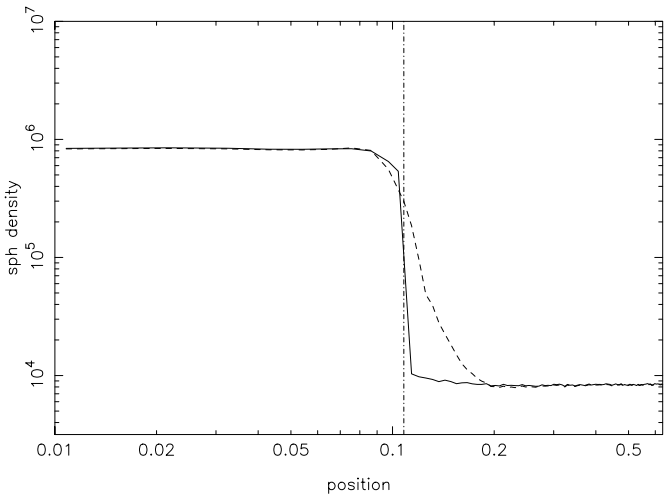

Figure 5. SPH estimation of the density across a density contrast of $\rho_l/\rho_r = 100$, which occurs at $r = 0.108$. Results from our new algorithm are shown as a solid line, while the results from the algorithm of T98 are shown as a dashed line. All units are code units.

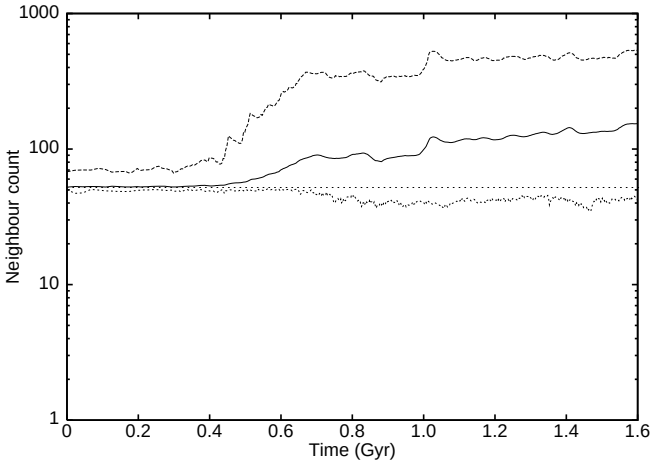

Figure 6. The maximum (dashed line), minimum (densely dotted line), average (solid line) and desired $N_{\rm SPH}$ (sparsely dotted line) weighted neighbour counts for the rotating cloud collapse problem. 1736 particles of both dark matter and gas are used. The increase in the average and maximum neighbour counts after $t \sim 4 \times 10^8$ years is due to the minimum smoothing length limit being reached.

~ 0.5 code units of the clump. At this point the particle has over 230 physical neighbours, 204 of which comprise the cold clump (although the weighted neighbour count from Equation 7 is almost exactly 32, as desired). Although individual cold particles only give a small contribution to Equation 10, the combined contribution is enough to make a noticeable increase in the estimate of the density.

Figure 5 shows the SPH estimate of the density profile across the boundary between two regions of different density, and demonstrates the sharpness with which density contrasts can be resolved by our method. To create the high density region we first evolve a cubical volume of gas at constant temperature, to ensure a relaxed particle distribution. We then extract a spherical volume and compress it radially to achieve the desired density. This is then inserted back into the cubical simulation volume and the particles are allowed to move at constant radius from the centre of the box for a few time-steps to ensure a fully stable initial state. Here the sphere has a radius $r = 0.108$ in code units, and is 100 times more dense than the surrounding gas, with the temperature again set so that the two regions are in pressure equilibrium.

Away from the boundary both methods correctly estimate the density, as we would expect. However, the standard implementation of SPH clearly overestimates the density close to the dense region, whereas the new algorithm gives a density contrast that is much sharper. On the high-density side of the boundary the differences are less pronounced. Under these circumstances our density-weighting method behaves in a very similar way to the method of HK89, as although low-density neighbours count double in the weighting, the Lagrangian nature of SPH means that the majority of the neighbours are in the high-density sphere and are weighted equally. As the particle distribution is inhomogeneous on the surface of the sphere, a surface particle has to search further to find its compliment of neighbours than a particle within the sphere, resulting in h increasing close to the boundary, and under such circumstances both methods will decrease their estimate of the density. While this is not ideal — we would like the density contrast to be sharp on both sides of the boundary — cold, high-density particles do not encounter problems from having their density underestimated, while it is far more important that hot particles have their density correctly estimated.

In order to ensure our new algorithm remains stable in the presence of sharp density contrasts, we use the rotating cloud collapse test described in T98. In this test a spherical cloud of dark matter and gas is set in solid-body rotation, and gravitational collapse combined with radiative cooling leads to a rotationally supported gaseous disc within a virialised dark matter halo. Following this collapse represents a challenging problem for any h-update algorithm, as the geometry rapidly changes from three to two dimensions and local densities can increase rapidly. Following T98, the initial radius of the gas cloud is 100 kpc and the total mass of dark matter and gas is $10^{12} M_\odot$. 1736 particles of dark matter and gas are used, and the gravitational softening length of both species is set as 2 kpc. Results from our algorithm are shown in Figure 6. Ideally the weighted number count would remain constant at $N_i = 52$ for each particle (we use this value, rather than $N_i = 32$ used elsewhere, for easy comparison with T98). Until a time $t \sim 4 \times 10^8$ years the scatter around the desired value is reasonable, with the minimum neighbour count being only slightly less than N_i and the maximum being at most $\sim 33\%$ too high. After this time the average and maximum neighbour counts increase rapidly. This is a result of the smoothing length not being allowed to decrease below the gravitational softening length, and once this limit is reached the neighbour count will rise as the collapse continues. The minimum neighbour remains in the range $\sim 30 - 50$ throughout the collapse, and demon-

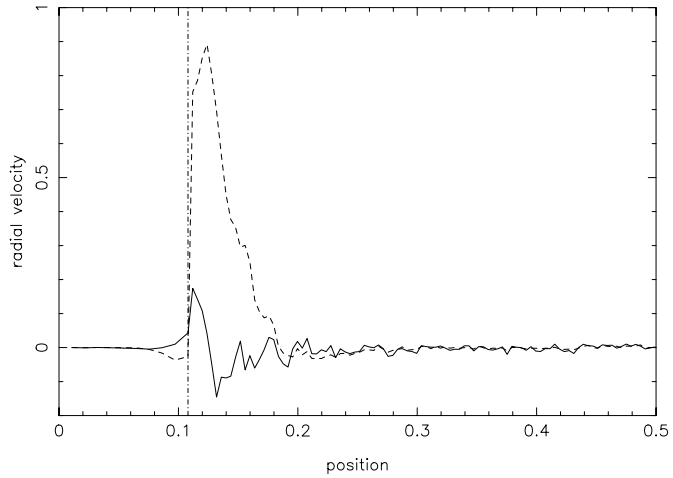

Figure 7. Average radial velocity after 10 time-steps across a density contrast $\rho_h/\rho_l = 100$, which occurs at $r = 0.108$. Results from our code are shown as a solid line, and results from the code of T98 are shown as a dashed line

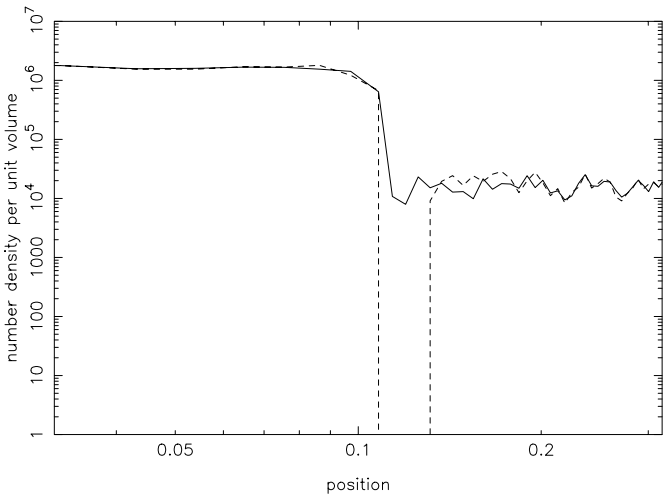

Figure 8. Number density of particles per unit volume after 25 time-steps across a density contrast $\rho_h/\rho_l = 100$, which occurs at $r = 0.108$. Results from our code are shown as a solid line, and results from the code of T98 are shown as a dashed line. The line marking the boundary between the two regions has been omitted for clarity. The empty region around the dense central clump can be clearly seen.

strates none of the instabilities that the affect the HK89 algorithm.

3.3 Two phase

In addition to excessive cooling, unphysical forces can also occur in the presence of steep density gradients. In implementations of SPH which try to keep the number of neighbours constant, a particle near a density gradient will find many, if not all, of its neighbours in the region of higher density. The pressure gradient at the particle will therefore be highly asymmetric, leading, from Equation 12, to a force that acts to push the particle away from the high density region. The strength of this force will depend on the magnitude of the density contrast, saturating once the particle finds all its neighbours in the high density region, and a dense clump of gas will therefore rapidly empty the surrounding region of particles.

We can see the effect of this asymmetric pressure gradient in Figure 7. Here, we plot the radial velocities after 10 time-steps of particles in or near the dense clump examined in the previous section. The scatter in velocity due to thermal motion of the hot gas is around ± 0.05 in both cases. The standard SPH code produces a large outward velocity in the hot gas, which evacuates a space between the two phases within a few tens of time-steps. This effect can be clearly seen in Figure 8, where the number density of particles drops to zero between $0.108 \leq r \leq 0.13$. While our method also produces excess velocities at the boundary, implying that the spurious pressure gradient has still not been completely eliminated, the magnitude of the outward velocity has been greatly reduced and the effect is far less systematic.

3.4 Drag

Drag resulting from gas dynamical forces is an important factor in simulations of cosmological structure formation, as incorrectly estimating the drag can bias both the distribution of matter in clusters and the size and number of objects formed. Frenk et al. (1996) have suggested that excessive drag can worsen the overmerging problem seen in N-body simulations, and TCP99 have shown that standard implementations of SPH can significantly overestimate the drag on a cold clump of gas moving through hot gas representative of the intracluster medium. This excess drag is caused by accretion of gas from the ICM on to a shell around the clump, where it is held by forces arising from the miscalculation of the pressure gradient around the clump (a discussion of this effect can be found in TCP99). This accretion leads to an increase in the effective radius of the clump, and hence the drag. This drag is most severe when the clump is moving subsonically, and at higher velocities the accretion of gas decreases, largely vanishing when the Mach number $\mathcal{M} \geq 2$.

In order to examine the drag introduced by our implementation of SPH, we consider the case of a clump of cold gas initially at rest in a stream of fast moving, diffuse gas (this is identical to the method of TCP99, except we work in the rest-frame of the cold clump). Assuming collisions are inelastic, the clump will be accelerated to the flow velocity v_0 at a rate

$$v = v_0 \left[\frac{e^{kt} - 1}{e^{kt} + 1} \right] \tag{36}$$

where k is a constant

$$k = \frac{2\pi r^2 \rho_0 v_0}{M} \tag{37}$$

in which ρ_0 is the density of the diffuse gas, v_0 the flow

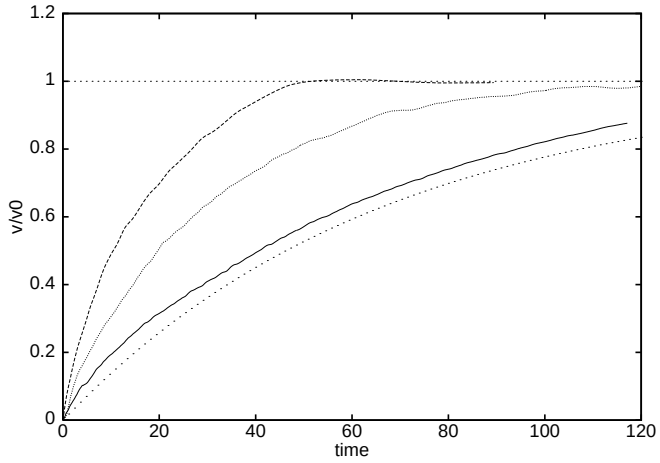

Figure 9. Rate of acceleration of a dense clump in a flow with Mach number 0.5. Results from our code are shown as a solid line, results from T98 are shown as a dashed line, results from CTP95 are shown as a densely dotted line and the prediction of Equation 36 are shown as a sparsely dotted line. All codes produce an excess drag.

velocity, r is the radius of the clump and M is the mass of the clump (all in code units). For our tests $M = 50$, $r = 0.5$, the velocity and density of the flow are set to unity and the Mach number of the flow is determined by setting the temperature of the gas as required. We use a Mach number $\mathcal{M} \sim 0.5$ here, which is well inside the regime in which TCP99 show that drag becomes excessive. Figure 9 compares the results from our new code with those obtained the codes of CTP95 and T98 (the code used by TCP99 is essentially the same as that used in T98). The results of our code are clearly an improvement, being close to the prediction of Equation 36. This is due to the elimination of the accretion that occurs in the other codes, as the asymmetric pressure gradients causing accretion are greatly reduced by our method. The difference between CTP95 and T98 is mainly a result of the kernel smoothing used in T98, which is shown in TCP99 to further increase the effective cross section of a dense clump. At higher Mach numbers the differences between the codes are less pronounced as the accretion decreases once $\mathcal{M} > 1$, although T98 continues to give the largest drag of the three codes.

3.5 Multiphase Cooling Flows

Clusters of galaxies contain large quantities of hot, X-ray emitting gas, often concentrated around the most massive galaxy in the cluster. In $\sim 70\% - 90\%$ of cases, gas in the centre of the cluster has a radiative cooling time less than the Hubble time, H_0^{-1} (Edge, Stewart & Fabian 1992; White, Jones & Forman 1997), and as this gas cools surrounding gas will move inwards to maintain pressure support, initiating a large-scale motion known as a cooling flow (see Fabian 1994 for a review). The mass deposition rate can be as high as $10^3 M_\odot \mathrm{yr}^{-1}$ (Fabian et al. 1985), and is often observed to vary with radius roughly as $\dot{M}(< r) \propto r$ within the radius r_{cool} in which the cooling time is less than a Hubble time (e.g. Thomas, Fabian and Nulsen 1987, hereafter TFN87). This is generally taken as evidence for a multiphase flow, in which thermal instability is causing the denser gas to cool out of the flow at larger radii.

Modelling a multiphase flow is impossible with the usual implementation of SPH as density is a locally averaged quantity, making the flow inherently single phase. In contrast, our method allows a wide range of densities, provided that a local pressure equilibrium exists. This is a reasonable assumption for particles with temperatures above 10^6K, which will have cooling times much greater than the local sound crossing time (Nulsen, 1988). Particles below 10^6K will cool to 10^4K within a few time-steps, at which point they are removed from the flow.

To test the ability of our code to model a fully multiphase environment, we examine a simple constant-pressure, spherically-symmetric cooling flow. The distribution of phases in the flow is described by the fractional volume distribution $f(\rho, r)$ introduced by Nulsen (1986, hereafter N86), where $f\mathrm{d}\rho$ is the fractional volume occupied by phases in the density range ρ to $\rho + \mathrm{d}\rho$. N86 considered many analytic forms for f. Here, we take

$$f(\rho, r) = \frac{(3-\alpha)}{\rho_0} \left(\frac{\rho}{\rho_0} \right)^{-(4-\alpha)} \qquad \rho > \rho_0 \tag{38}$$

with ρ_0 being a minimum density and α the temperature dependence of the cooling function $\Lambda \propto T^\alpha$. For the purposes of this test we replace the Sutherland & Dopita (1993) cooling function with a pure power law in which $\alpha = 0.5$. Then Equation 38 can be integrated (N86) and gives a mass deposition profile

$$\dot{M} \propto r^\eta \tag{39}$$

where

$$\eta = \frac{3(2-\alpha)}{(5-2\alpha)} = \frac{9}{8}. \tag{40}$$

Particles are placed randomly within a cubical simulation of volume $(200\mathrm{kpc})^3$, and are then allowed to evolve at constant temperature until spurious fluctuations arising from the initial particle distribution have died away. Particles are then ordered in terms of their distance from the centre of the box, and translated radially so as to match the mass profile given by

$$M \propto \rho_0(r) r^3 \tag{41}$$

where the density profile

$$\rho_0(r) \propto r^{-\frac{3}{(5-2\alpha)}} \propto r^{-3/4} \tag{42}$$

is derived in TFN87. Particles translated outside the bounds of the box are discarded. Particle densities are drawn at random from the volume fraction distribution given by Equation 38, with particle temperatures set so as to maintain constant pressure. Here, the outer temperature is $T \sim 5 \times 10^7 K$, the inner temperature $T \sim 10^6 K$, the central density is $0.1\mathrm{cm}^{-3}$ and the average outer density is $\sim 5 \times 10^{-3}\mathrm{cm}^{-3}$. A total of 20252 particles are used.

Figure 10 shows the mass deposition profile $\dot{M}(< r)$, produced by the multiphase method after 500 timesteps. Roughly 11% of the gas has cooled from the flow. The line marks a least-squares fit to the data, with slope $\eta =$

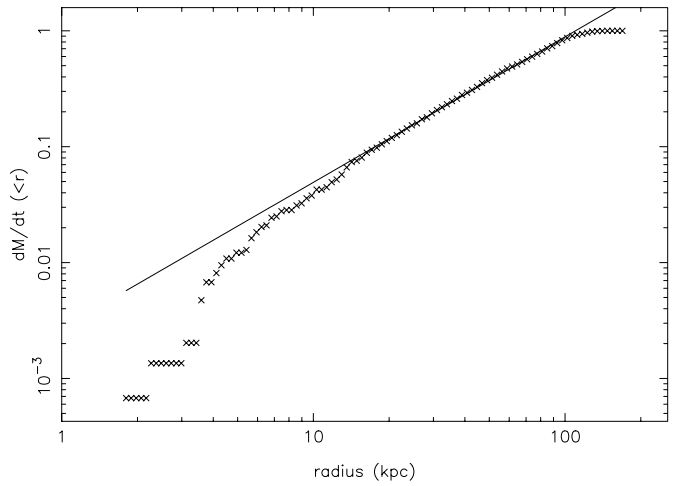

Figure 10. Mass deposition profile produced by the multiphase code after 500 timesteps. Approximately 11% of the gas has cooled out of the flow. The solid line represents a least squares fit to the profile between 15kpc $< r <$ 100kpc, and has a slope 1.26 ± 0.01.

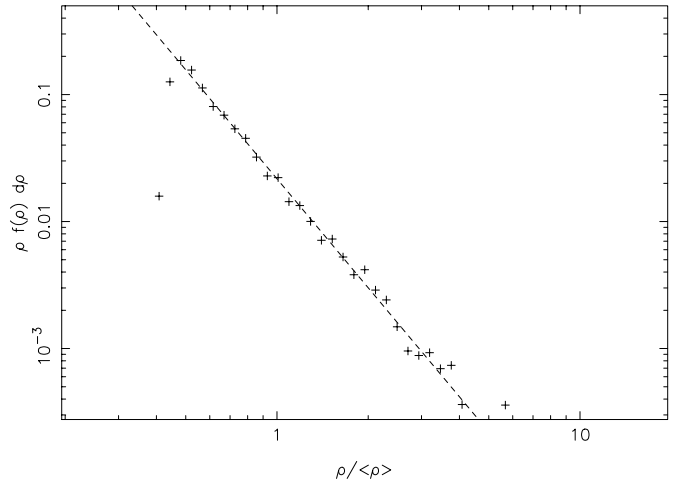

Figure 11. Mass distribution function $\rho f \mathrm{d}\rho$ of the uncooled gas at radii 50kpc $< r <$ 60kpc for the multiphase code. We would expect the distribution to be unchanged from the initial distribution given by Equation 38, with the points on a power-law $\propto \rho^{-2.5}$. The dashed line represents a least-squares fit (excluding the first two points), and has a slope -2.75 ± 0.06.

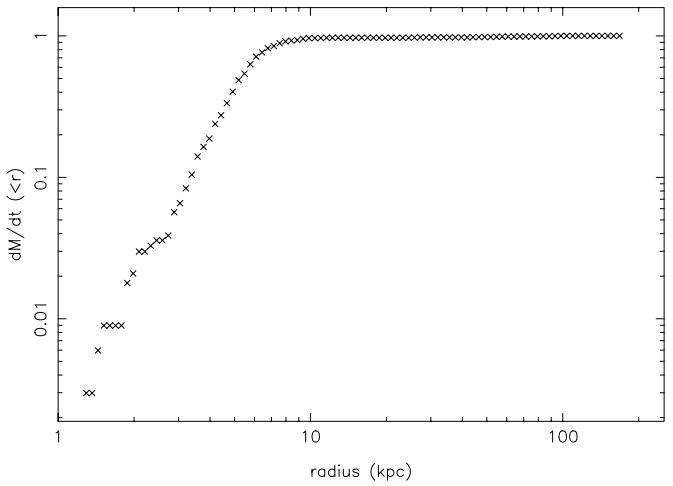

Figure 12. Mass deposition profile produced by the standard implementation of SPH after 500 timesteps. Approximately 5% of the gas has cooled out of the flow. Virtually all the matter has been deposited within the central ~ 8 kpc, as would be expected of a single-phase cooling flow.

1.26 ± 0.01. The points within 15kpc of the centre of the flow have been excluded from this fit, as there are too few particles here for the mass deposition profile to be well sampled, as have particles with $r >$ 100kpc which lie in the corners of the cubical simulation volume. The slope is slightly steeper than the theoretical index of $\eta = 9/8$. Figure 11 shows the mass distribution function $\rho f \mathrm{d}\rho$ for particles at radii of between 50 and 60 kpc. In theory we would expect the distribution of phases given by Equation 38 to remain unchanged with time, giving $\rho f \mathrm{d}\rho \propto \rho^{-2.5}$. The dashed line represents a least-squares fit to the data, with gradient -2.75 ± 0.06. This is again steeper than we would expect. This is probably due to the phases not comoving, an assumption made in N86. There is no condition in our code to enforce this, and Equation 12 implies that high-density particles will recieve a smaller pressure force than low-density ones. The artificial viscosity will limit the degree to which particles can interpenetrate, ensuring that the flow is largely comoving, but it may not be sufficient to ensure that no slippage occurs. Applying a large bulk viscosity term in Equation 27 forces the particles to comove, and flattens both slopes towards their theoretical values. However, this is not suitable for general application as it degrades the shock capturing ability of the method.

The mass deposition profile produced by the standard implementation of SPH is shown in Figure 12. 500 timesteps have passed and this time about 5% of the gas has cooled. In contrast with the multiphase results, this implementation produces a mass deposition profile that is centrally concentrated, as would be expected from a single-phase flow. This is supported by the mass distribution function, which is plotted in Figure 13. The gas has clearly evolved back to a single-phase state, with all particles having a density close to the mean, and no trace of the original density distribution remains. In addition, the gradient of the density profile has steepened from an initial value of $\rho \propto r^{-0.75}$ (as given

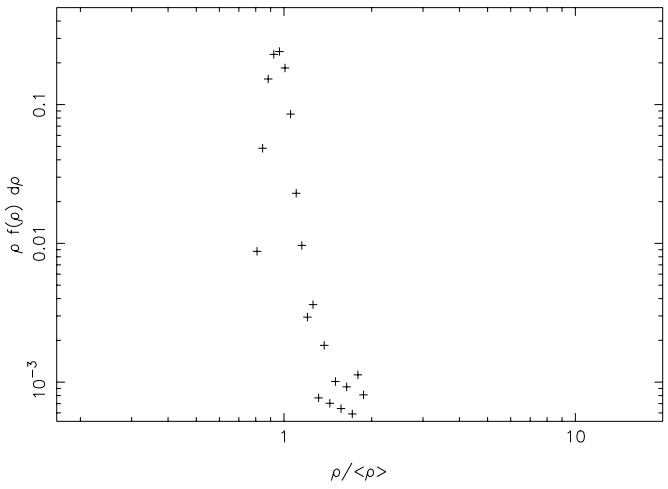

Figure 13. Mass distribution function $\rho f \mathrm{d}\rho$ of the uncooled gas at radii 50kpc $< r <$ 60kpc for the standard implementation of SPH. All particles have densities close to the mean, and there is no trace of the original density distribution.

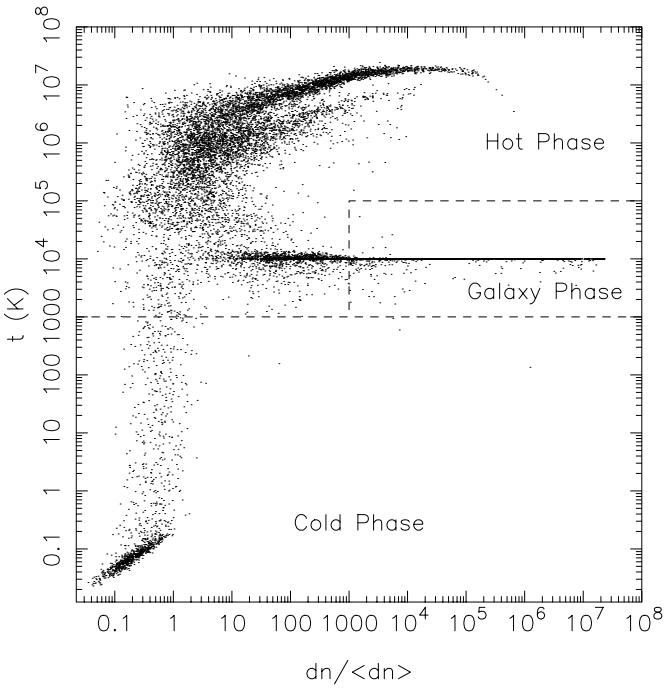

Figure 14. The temperature-density phase diagram of the gas at $z = 0$ in the multiphase cluster-formation simulation. Density is in units of the mean density. The diagram is divided into three phases; the *cold* phase, containing gas with $T < 10^3 K$, the *galaxy* phase, containing gas which is overdense by at least a factor of 10^3 and has a temperature of $10^3\mathrm{K} \leq T \leq 10^5\mathrm{K}$ and the *hot* phase, containing all gas with a temperature of $T \geq 10^5\mathrm{K}$ and the gas with $T \geq 10^3\mathrm{K}$ which is not sufficiently overdense to be considered part of the galaxy phase.

by Equation 42) to $\rho \propto r^{-1.15\pm0.03}$, close to the theoretical single-phase value of $\rho \propto r^{-1.2}$ (Thomas, 1988).

When compared to the standard implementation of SPH, it is clear that our method performs well. Both the mass deposition profile and the distribution of densities in the flow are close to the theoretical values, whereas the standard implementation fails to reproduce the properties of the flow correctly.

3.6 Cosmological Galaxy Formation

Our final test involves a simulation of the formation of a cluster of galaxies. We use the initial conditions from the fiducial simulation of Kay et al. (1999), who used it to test in detail the effect of varying a number of numerical and physical parameters. The simulation uses the standard cold dark matter (SCDM) cosmology, with $\Omega = 1$, $\Lambda = 0$ and $h = 0.5$[‡]. The baryon fraction was set from primordial nucleosynthesis constraints, $\Omega_b h^2 = 0.015$ (Copi, Schramm & Turner 1995), and an unevolving gas metallicity of $0.5 Z_\odot$ was used. The initial fluctuation amplitude was set so that the model produces the same number density of rich clusters as is observed today, with σ_8, the present-day linear rms fluctuation on a scale of $8h^{-1}$Mpc, set to 0.6 (Eke, Cole & Frenk 1996; Vianna & Liddle 1996). Until $z \sim 1$ we adopt a comoving β-spline gravitational softening equivalent to a Plummer softening of $20h^{-1}$kpc, after which it is switched to a fixed physical softening of $\sim 10\ h^{-1}$kpc. The minimum SPH resolution is set to match the constraints imposed by the gravitational softening. 32^3 particles of both dark matter and gas were used, giving a mass per particle of $8 \times 10^9 h^{-1} M_\odot$ for the dark matter and $5 \times 10^8 h^{-1} M_\odot$ for the gas. The simulation was started at $z \sim 24$ and was evolved to the present day.

‡ $H_0 = 100h\,\mathrm{kms}^{-1}\mathrm{Mpc}^{-1}$

Our method is based on the assumption that a local pressure equilibrium exists, which is not always valid for cosmological simulations. Within dark matter halos, an approximate pressure equilibrium does exist, and the method works well. However, gas occupying dark matter voids typically has temperatures on the order of a few Kelvin, and is far from pressure equilibrium with the hot gas on the outer edges of halos which is at a similar overdensity but at temperatures in excess of 10^5K. When a cold particle encounters a hot halo particle, for example in the early stages of its own gravitational collapse into the halo, the hot neighbour will make an overwhelming contribution to the estimate of the pressure given by Equation 10, resulting in the particle having its density overestimated, potentially by many orders of magnitude. This effect decreases as the particle is shock heated towards the virial temperature, but results in the properties of very cold gas being miscalculated. In order to avoid this problem we use the standard implementation of SPH for uncollapsed gas, switching to our method once the particle has been shock heated above 10^4K for the first time.

Figures 14 and 15 illustrate the temperature-density distribution of baryonic matter at $z = 0$ produced by the multiphase and standard codes. Following Kay et al., we have divided the gas into three phases; a *cold* phase containing all gas with $T < 10^3$K, a *galaxy* phase containing

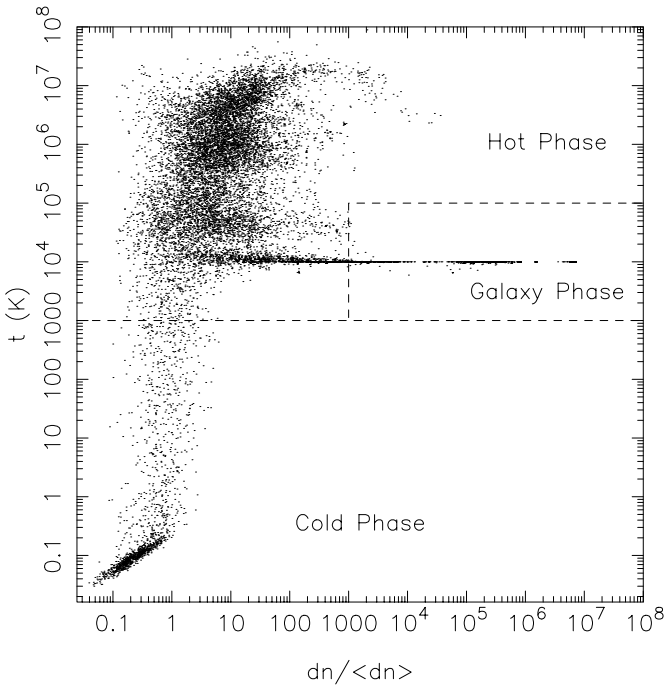

Figure 15. The temperature-density phase diagram of the gas at $z = 0$ in the multiphase cluster-formation simulation. Density is in units of the mean density. The phases are defined in the same way as in Figure 14.

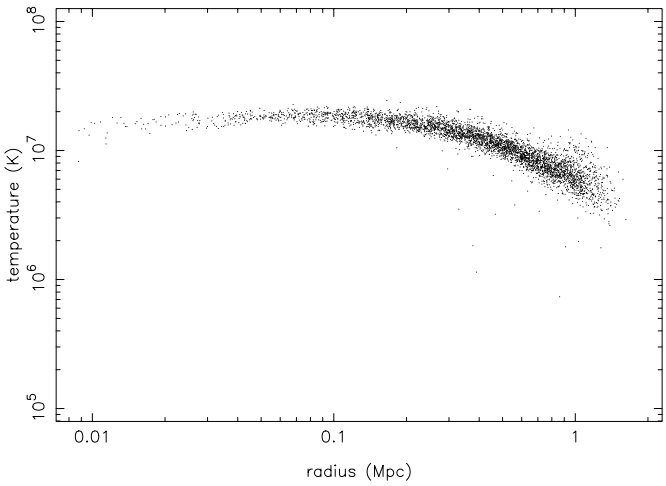

Figure 16. Radial temperature profile through the hot gas halo surrounding the largest galaxy found in the multiphase simulation.

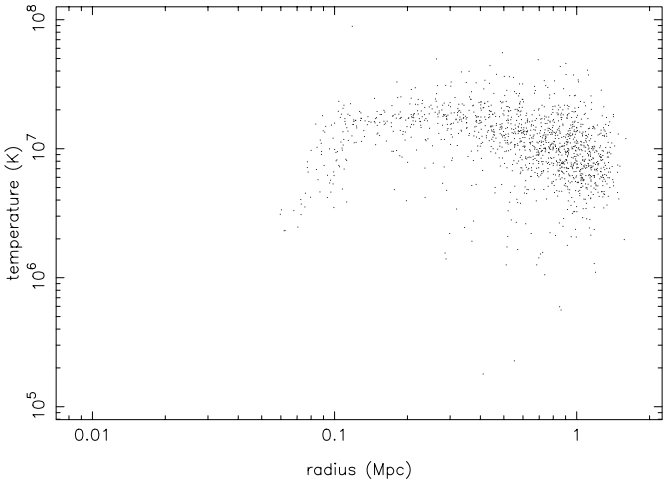

Figure 17. Radial temperature profile through the hot gas halo surrounding the largest galaxy found in the single phase simulation.

gas which is overdense by at least a factor of 10^3 and has a temperature of $10^3\mathrm{K} \leq T \leq 10^5\mathrm{K}$ and a *hot* phase which includes all gas with a temperature of $T \geq 10^5\mathrm{K}$ and the gas with $T \geq 10^3\mathrm{K}$ which is not sufficiently overdense to be considered part of the galaxy phase. Most of the particles in the cold phase are still in free expansion and are cooling adiabatically, with the remainder part of a plume of particles undergoing shock heating.

Almost all the particles in the galaxy phase lie along a horizontal line with $T = 10^4\mathrm{K}$, which marks the point at which the radiative cooling rate drops to zero. Most of these particles are in the form of dense clumps with a size similar to the gravitational softening length - we refer to these clumps as galaxies. The properties of these galaxies are calculating by first extracting all particles within the galaxy phase from the simulation volume and then running a 'friends-of-friends' group finder (Davis et al. 1985). The most significant difference between the two simulations is in the mass of the largest galaxy, which is nearly 50% more massive in the single-phase simulation. Although the galaxies are less massive in the multiphase simulations, there is slightly more gas in the galaxy phase, with the additional gas distributed throughout the dark matter halos. This gas is not present in the standard simulations, and is a result of the amplification of density fluctuations in the gas by the multiphase method, leading to the gas cooling out of the hot phase and being deposited throughout the halo.

The hot phase consists of particles that have been shock heated during gravitational collapse, with the bulk kinetic energy of the gas being converted to heat. Figure 14 shows a significant quantity of hot ($T > 10^7\mathrm{K}$), high-density ($\rho/\langle\rho\rangle > 10^4$) gas which is not present in Figure 15 but *is* seen in the single-phase simulations when radiative cooling is not allowed. This gas is located near the centre of large dark matter halos, close to the central galaxy, and overestimation of the already high gas density by the standard method leads to the gas rapidly cooling and being accreted by the galaxy. In contrast, the multiphase method correctly estimates the density of the gas, resulting in a slower cooling rate and the gas remaining at high temperatures throughout the halo. This effect can be seen in more detail in Figures 16 and 17, which show the radial temperature profile of the gas around the most massive galaxy found in the simulation volume. The size of the galaxy is on the order of the softening length, $\sim 10h^{-1}\mathrm{kpc}$, and is not shown here. The results from

the standard implementation clearly show two of the problems inherent in the method. Firstly, particle temperatures drop sharply within $r < 100$kpc - this is clear evidence for overcooling. No such effect is visible in Figure 16 and the lack of overcooling in our method is probably the principle reason for the difference in mass of the largest objects in the two simulations. Secondly, there is a complete absence of particles at radii $r < 50$kpc, whereas particles are found all the way in to $r \sim 10$kpc in the multiphase simulations. This is an example of the effect examined in Section 3.3, with particles close to the central galaxy being forced away by an artificially asymmetric pressure gradient in the single-phase method.

4 DISCUSSION AND CONCLUSIONS

We have presented a multiphase implementation of Smoothed-Particle Hydrodynamics (SPH), along with a number of tests to compare the performance of our method with standard implementations of SPH. The usual SPH formalism assumes that density is a smooth quantity, varying negligably on distances on the order of a typical smoothing length. This is clearly not true in many situations in which SPH is applied, such as simulations of galaxy formation, in which large density contrasts are present. However, the pressure of the gas is expected to be a much smoother quantity because in almost all situations the sound-crossing time is shorter than the flow time across the smoothing sphere. We therefore summate the local pressure at each particle, and calculate the density from the equation of state.

One situation in which our assumption will definitely not be true is in the presence of shocks, in which density variations are generally smaller than the variations in pressure. Section 3.1 demonstrates that our method handles shocks comparably with the standard SPH implementation, largely because the gas dynamics are dominated by the artificial viscosity under such situations and the choice of hydrodynamical method is of lesser importance. In Section 3.2 we examine the degree to which steep density gradients can be resolved by the two methods. Standard implementations of SPH are shown to severely overestimate the density of particles close to a region of high density, while these particles have their density correctly estimated by our method. The smoothing-length update algorithm used in our code is shown to remain stable during a the collapse of a rotating cloud of gas and dark matter, a test that T98 show causes the HK89 algorithm to become unstable. In addition, we show in Section 3.3 that unphysical forces can occur in the presence of steep density gradients, and while such forces are not completely eliminated by our method, they are greatly reduced. Section 3.4 examines the drag introduced by our implementation of SPH. We find that at low Mach numbers drag is greatly reduced compared to the SPH implementations of CTP95 and T98, while at higher velocities the results are in broad agreement with the findings of TCP99, depending mainly on the choice of smoothing kernel symmetrization.

In Section 3.5 we examine a simple spherically-symmetric, constant pressure cooling flow. The fractional volume distribution $f\mathrm{d}\rho$ of phases within the flow is taken to be a pure power-law, which is shown by N86 to remain unchanged with time and deposit mass as $\dot{M}(< r) \propto r^{9/8}$. The standard implementation of SPH is shown to be unable to reproduce the expected behaviour of this cooling flow, with conditions rapidly returning to a single-phase state. Our code performs well, although the gradient of both the mass distribution $\rho f\mathrm{d}\rho$ and the mass deposition profile $\dot{M}$ are too steep. This is probably due to phases not comoving in the flow, which is an assumption made in N86. Application of a large bulk viscosity to force particles to comove appears to reduce the problem, although this is not a suitable for application generally as it results in the shock capturing ability of the code being significantly degraded.

In Section 3.6 we examine the formation of a cluster of galaxies. The idealised problems examined in Sections 3.2 and 3.3 are shown to have real analogues in the simulation using the standard SPH implementation, with overcooling resulting from overestimating the density of halo gas being clearly visible, and halo gas being forced away from the central galaxy. No such effects are visible in the simulation using our method. The lack of overcooling is also apparent in the masses of the galaxies formed, with the largest galaxy being nearly 50% more massive in the single-phase simulation, in agreement with the findings of Pearce et al. (1999), who found that decoupling the galaxy from the hot halo gas produced a similar effect. A further difference between our results and those using the standard implementation of SPH is the presence of gas at 10^4K in the halos around galaxies, resulting from the amplification of small density variations in the gas. The temperature of the gas is arbitrary, as the gas cannot cool further, but is an indication of the multiphase nature of the intracluster gas in our simulations.

Our method is an alternative to the standard formulation of SPH. In simulations without large density contrasts, the two give very similar results. However it represents a significant improvement over the standard implementation of SPH when the gas component cannot be assumed to be a single-phase fluid, such as galaxy formation and cluster formation. In addition, fully multiphase fluid flow can be modelled, allowing SPH to be applied to simulations of cooling flows and the intracluster medium.

Acknowledgments

BWR acknowledges the support of a PPARC postgraduate studentship. PAT is a PPARC Lecturer Fellow. The authors would like to thank Rob Thacker for supplying initial conditions used in Section 3.2 and Scott Kay for those used in Section 3.6.

References

Balsara D. W., 1995, J. Chem. Phys., 121, 357
Bertschinger, E., 1998, ARA&A, 36, 599
Bhattal A. S., Francis N., Watkins S. J., Whitworth A. P., 1998, MNRAS, 297, 435
Blanton M., Cen R., Ostriker J. P., Strauss M. A., 1999, ApJ, 522, 590
Collela P., Woodward P. R., 1984, J. Comp. Phys., 54, 174
Copi C. J., Schramm D. N., Turner M. S., 1995, ApJ, 455, 95

Couchman H. M. P., 1991, ApJ, 368, 23
Couchman H. M. P., Thomas P. A., Pearce F. R., 1995, ApJ, 452, 797 (CTP95)
Davis M., Efstatiou G., Frenk C. S., White S. D. M., 1985, ApJ, 292, 371
Edge A. C., Stewart G. C., Fabian A. C., 1992, MNRAS, 258, 177
Eke V. R., Cole S., Frenk C. S., 1996, MNRAS, 282, 263
Evrard A. E., 1988, MNRAS, 235, 911
Fabian A. C., 1994, ARA&A, 32, 277
Fabian A. C., Arnaud K. A., Nulsen P. E. J., Watson M. G. Stewart G. C., McHardy I., Smith A., Cooke B., Elvis M., Mushotzky R. F., 1985, MNRAS, 216, 923
Flebbe O., Münzel S., Herold H., Riffert H, Ruder H., 1994, ApJ, 431, 754
Frenk C. S., Evrard A. E., White S. D. M., Summers F. J., 1996, ApJ, 472, 460
Gingold R. A., Monaghan J. J., 1977, MNRAS, 181, 375
Gingold R. A., Monaghan J. J., 1983, MNRAS, 204, 715
Hawley J. F., Smarr L. L., Wilson J. R., 1984, ApJ, 277, 296
Hernquist L., Katz N., 1989, ApJS, 70, 419 (HK89)
Hutchings R. M., Thomas P. A., 1999, Preprint astro-ph/9903320
Kay S. T., Pearce F. R., Jenkins A., Frenk C. S., White S. D. M., Thomas P. A., Couchman H. M. P., 1999, Preprint astro-ph/9908107
Lucy L. B., 1977, AJ, 82, 1013
Monaghan J. J., 1992, ARA&A, 30, 543
Monaghan J. J., Gingold R. A., 1983, J. Comp. Phys., 52, 375
Navarro J., Steinmetz M., 1997, ApJ, 478, 13
Nelson R. P., Papaloizou J. C. B., 1994, MNRAS, 270, 1
Nulsen P. E.J., 1986, MNRAS, 221, 377 (N86)
Nulsen P. E. J., 1988, in NATO ASI Cooling flows in clusters and galaxies, eds, Fabian A. C.. Kluwer, Dordrecht, p. 175
Pearce F. R., Jenkins A., Frenk C. S., Colberg J. M., Thomas P. A., Couchman H. M. P., White S. D. M., Efstathiou G., Peacock J. A., Nelson A. H. (The Virgo Consortium), 1999, ApJ, 521, 99
Rasio F. A., Shapiro S. L., 1991, ApJ, 377, 559
Shapiro P. R., Martel H., Villumsen J. V., Owen J. M., 1996, ApJS, 103, 269
Sod G. A., 1978, J. Comp. Phys., 27, 1
Steinmetz M., 1996, MNRAS, 278, 1005
Steinmetz M., Müller E., 1993, A&A, 268, 391
Sutherland R. S., Dopita M. A., 1993, ApJS, 88, 253
Thacker R., Tittley E. R., Pearce F. R., Couchman H. M. P., Thomas P. A., 1998, Preprint astro-ph/9809221 (T98)
Tittley E. R., Couchman H. M. P., Pearce F. R., 1999, Preprint astro-ph/9911017 (TCP99)
Thomas P.A., 1988, in NATO ASI Cooling flows in clusters and galaxies, eds, Fabian A.C.. Kluwer, Dordrecht, p. 361
Thomas P. A., Couchman H. M. P., 1992, MNRAS, 257, 11
Thomas P.A., Fabian A. C., Nulsen P. E. J. N., 1987, MNRAS, 228, 973 (TFN87)
Viana P. T. P., Liddle A. R., 1996, MNRAS, 281, 323
White D. A., Jones C., Forman W., 1997, MNRAS, 292, 419
Wood D., 1981, MNRAS, 194, 201

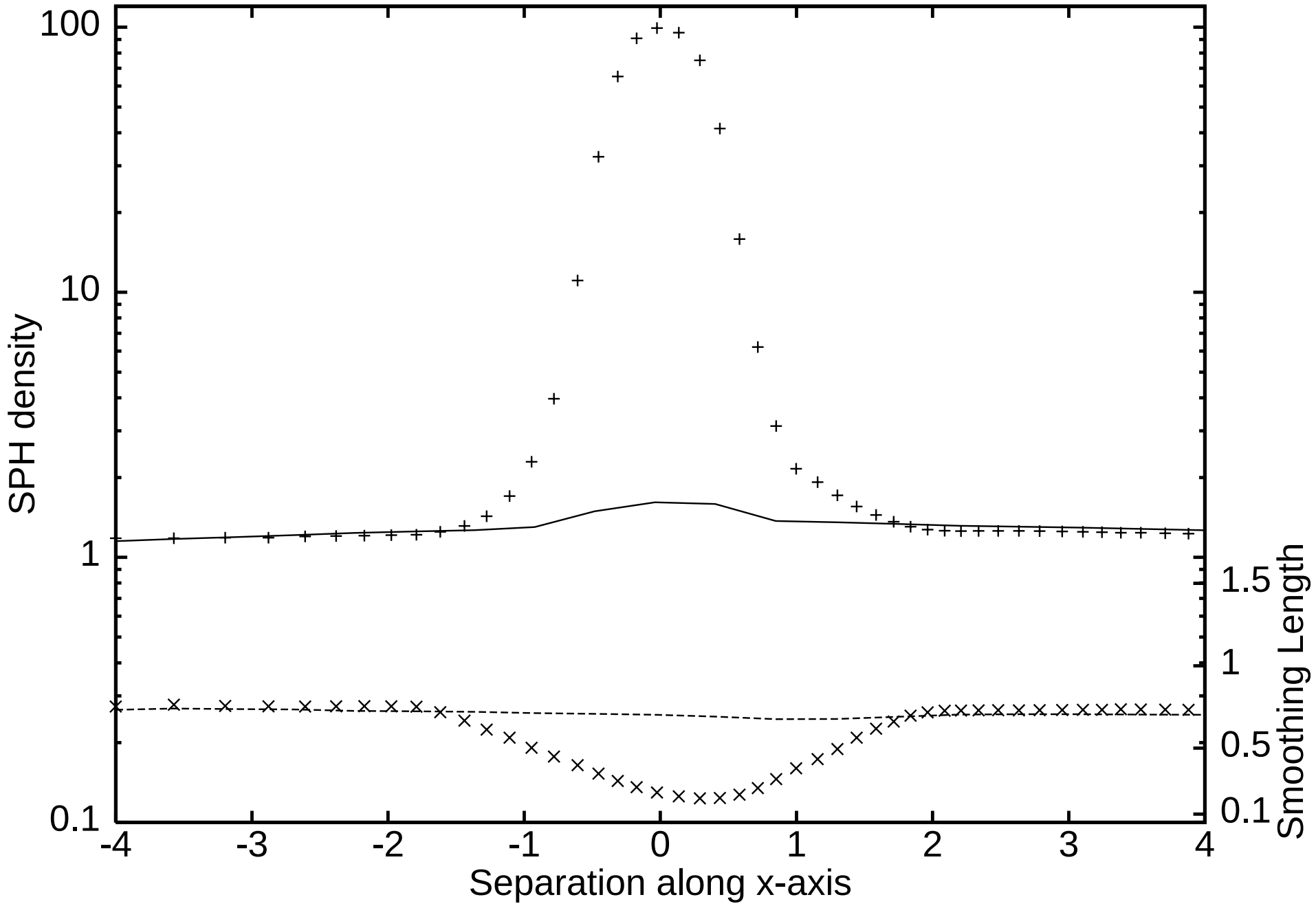
100
10
1
0.1
SPH density
-4
-3
-2
-1
0
1
2
3
4
Separation along x-axis
1.5
1
0.5
0.1
Smoothing Length

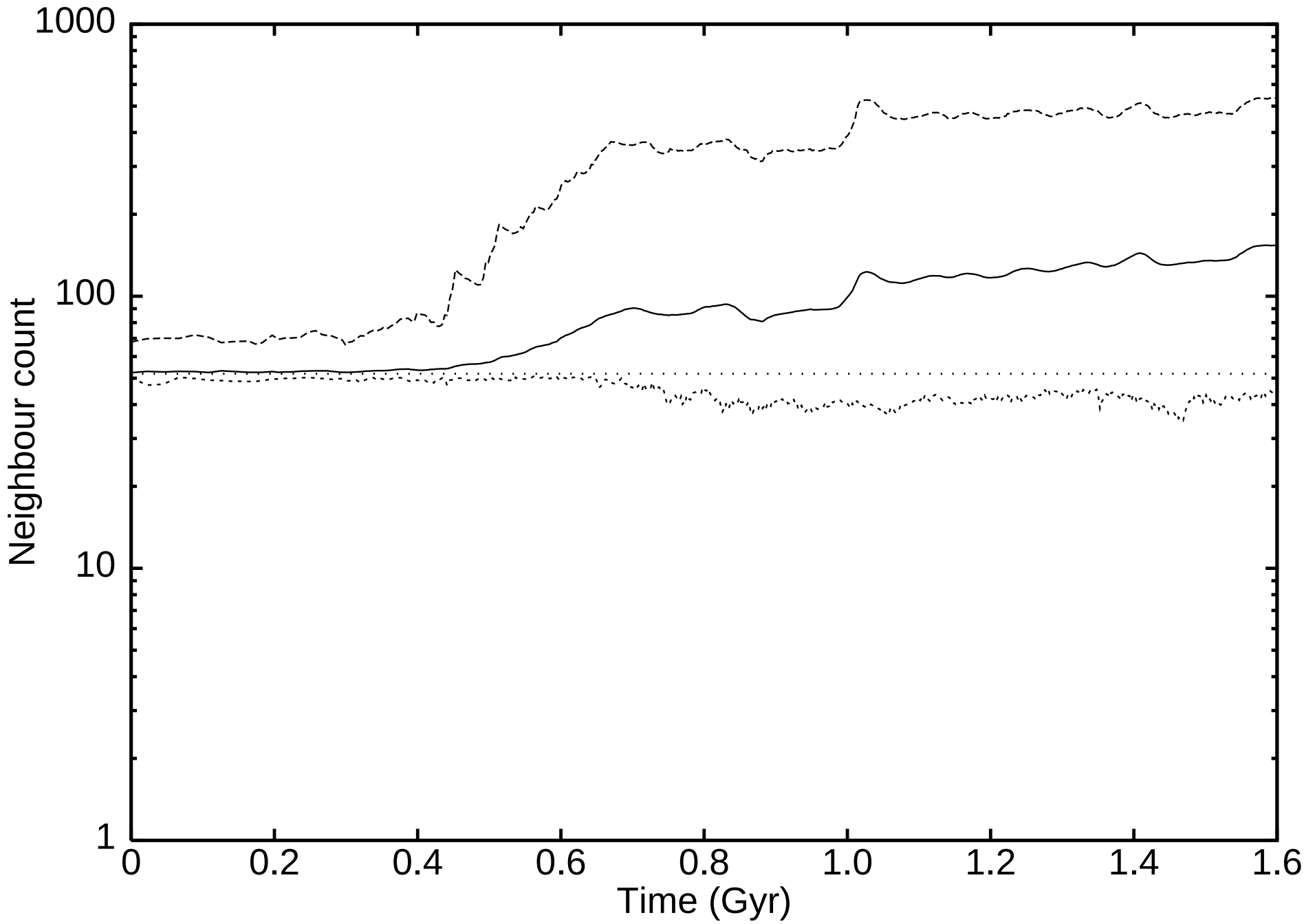
1000
100
10
1
Neighbour count
0
0.2
0.4
0.6
0.8
1.0
1.2
1.4
1.6
Time (Gyr)

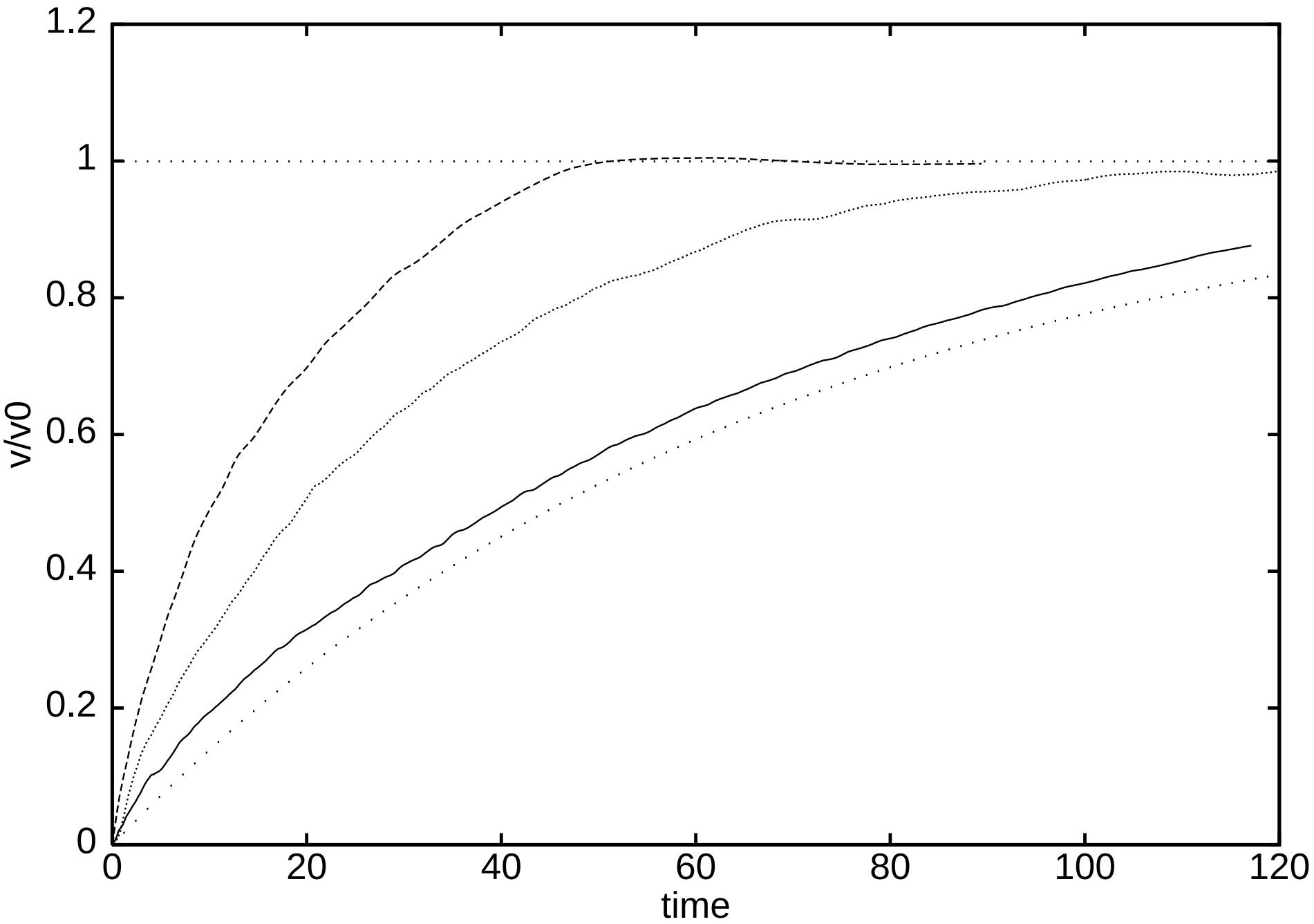
1.2
1
0.8
0.6
0.4
0.2
0
v/v0
0
20
40
60
80
100
120
time